

Cite this: *Chem. Sci.*, 2022, **13**, 5261

All publication charges for this article have been paid for by the Royal Society of Chemistry

Received 7th March 2022
Accepted 3rd April 2022

DOI: 10.1039/d2sc01342h
rsc.li/chemical-science

Introduction

The addition of an electron can significantly change the chemical and electronic nature of molecules.^{1,2} The extra electron ($+e^-$) populated in the antibonding orbital weakens the chemical bond,³ leading to reductive fragmentations that form a redox-active fragment and a highly stable coproduct.^{1,2} When the resulting active fragment has sufficient reducing power to reduce the reactant, electrocatalytic chain reactions can be triggered.^{1,2} Synthetic studies on such electron upconversions have focused on challenging chemical transformations.^{1,2,4-12} However, the advantages of electrons as a remote and accessible chemical input also show promise for the development of new dynamic host-guest systems,^{13,14} whereby electrocatalytic chain reactions enable guest molecule release,¹⁴⁻¹⁸ ultimately affording a one-electron switch using only a catalytic amount of electrons as the input dots.

Herein, we demonstrate electrocatalytic chain reactions capable of turning on charge-transfer (CT) complex formation, accompanied by solvent molecule release and redox-active anthraquinone formation, for the first time (Scheme 1).¹⁹ Quinone derivatives are important electron carriers widely

Catalytic electron drives host-guest recognition†

Yoshihiro Owatari, Shuta Iseki, Daiji Ogata and Junpei Yuasa *

Electron injection is demonstrated to trigger electrocatalytic chain reactions capable of releasing a solvent molecule and forming a redox active guest molecule. One-electron reduction of a hydroxy anthrone derivative ($\text{AQH-CH}_2\text{CN}$) results in the formation of an anthraquinone radical anion ($\text{AQ}^{\cdot-}$) and acetonitrile (CH_3CN). The resulting fragment of $\text{AQ}^{\cdot-}$ exhibits high stability under mild reducing conditions, and it has enough reducing power to reduce the reactant of $\text{AQH-CH}_2\text{CN}$. Hence, subsequent electron transfer from $\text{AQ}^{\cdot-}$ to $\text{AQH-CH}_2\text{CN}$ yields the secondary $\text{AQ}^{\cdot-}$ and CH_3CN , while the initial $\text{AQ}^{\cdot-}$ is subsequently oxidized to AQ . Overall, the reactants of $\text{AQH-CH}_2\text{CN}$ are completely converted into AQ and CH_3CN in sustainable electrocatalytic chain reactions. These electrocatalytic chain reactions are mild and sustainable, successfully achieving catalytic electron-triggered charge-transfer (CT) complex formation. Reactant $\text{AQH-CH}_2\text{CN}$ is non-planar, making it unsuitable for CT interaction with an electron donor host compound ($\text{U}_\text{H}\text{Ant}_2$) bearing parallel anthracene tweezers. However, conversion of $\text{AQH-CH}_2\text{CN}$ to planar electron acceptor AQ by the electrocatalytic chain reactions turns on CT interaction, generating a host CT complex with $\text{U}_\text{H}\text{Ant}_2$ ($\text{AQ} \subset \text{U}_\text{H}\text{Ant}_2$). Therefore, sustainable electrocatalytic chain reactions can control CT interactions using only a catalytic amount of electrons, ultimately affording a one-electron switch associated with catalytic electron-triggered turn-on molecular recognition.

distributed in nature,²⁰ and have recently been utilized as guest molecules in host-guest systems.^{18,21-23} Electron injection to a hydroxy anthrone derivative ($\text{AQH-CH}_2\text{CN}$) results in the formation of an anthraquinone radical anion ($\text{AQ}^{\cdot-}$) and a stable coproduct (acetonitrile, CH_3CN) [Scheme 1a]. Redox-active fragment $\text{AQ}^{\cdot-}$ has sufficient reducing power to reduce reactant $\text{AQH-CH}_2\text{CN}$ (Scheme 1b), which initiates the electrocatalytic chain reaction (Scheme 1a). This electron upconversion produces a much lower amount of energy (3.5 kcal mol⁻¹, 0.15 eV; Scheme 1b) compared with electron upconversions used for synthetic purposes (20–25 kcal mol⁻¹).² Even the redox-active fragment ($\text{AQ}^{\cdot-}$) is stable under mild reducing conditions, and the stable coproduct (CH_3CN) is a solvent molecule that has no impact on the electrocatalytic chain reaction. Therefore, the present electrocatalytic chain reactions are mild and sustainable, providing new opportunities for catalytic electron-triggered host-guest systems (Scheme 1c). Reactant $\text{AQH-CH}_2\text{CN}$ is non-planar, making it unsuitable for host-guest systems driven by CT interactions. However, the electrocatalytic chain reaction converts $\text{AQH-CH}_2\text{CN}$ to AQ , which is a planar electron-acceptor suitable for CT interactions, making turn-on generation of a host CT complex possible. Therefore, the sustainable electrocatalytic chain reactions demonstrated here can control host-guest molecular recognition using only a catalytic amount of electrons. This paves the way for a “one-electron switch” associated with catalytic electron-triggered turn-on molecular recognition (Scheme 2).

Department of Applied Chemistry, Tokyo University of Science, 1-3 Kagurazaka, Shinjuku, Tokyo 162-8601, Japan. E-mail: yuasaj@rs.tus.ac.jp; Fax: +81-3-72-6179

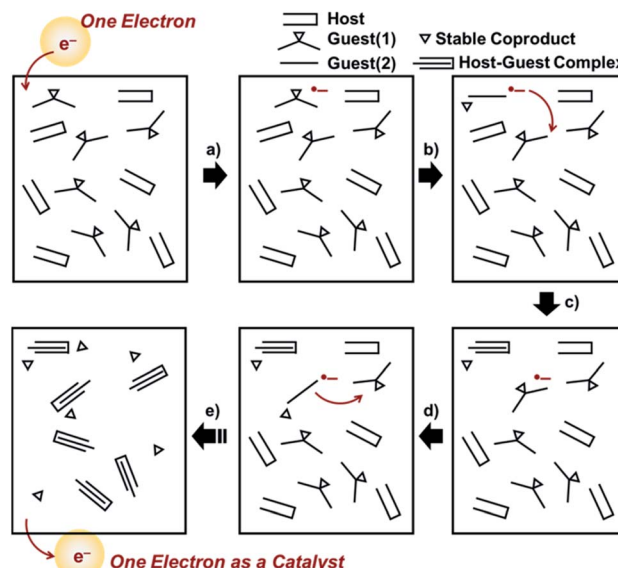
† Electronic supplementary information (ESI) available. CCDC 2096046. For ESI and crystallographic data in CIF or other electronic format see <https://doi.org/10.1039/d2sc01342h>



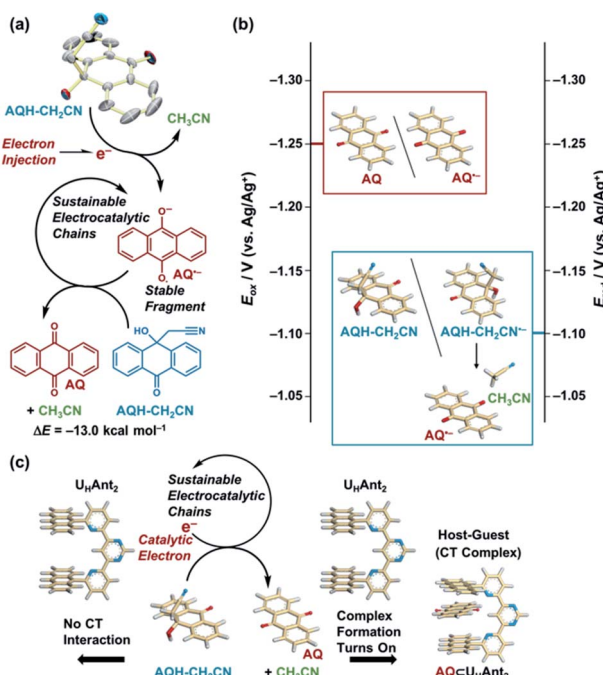
Results and discussion

The hydroxy anthrone derivative ($\text{AQH-CH}_2\text{CN}$)²⁴ was synthesized by solvolysis of anthraquinone (AQ) under strong basic conditions in acetonitrile (see the ESI†). The resulting $\text{AQH-CH}_2\text{CN}$ was successfully crystallized to reveal a C-C bond ($d_{\text{c-c}} = 1.56 \text{ \AA}$) between the CH_2CN moiety and the carbon atom of the anthrone ring at the connected position (Scheme 1a). Although that C-C bond is slightly longer than a conventional C-C bond ($\leq 1.54 \text{ \AA}$), it is not considered as a significant high-energy bond. Density functional theory (DFT) calculations [DFT/B3LYP-6-31G+(d,p)] predict that the dissociated product (*i.e.*, AQ + CH_3CN) is 13.0 kcal mol⁻¹ lower in energy than $\text{AQH-CH}_2\text{CN}$, while $\text{AQH-CH}_2\text{CN}$ itself is stable in the long term, thus indicating a relatively large activation barrier for the conversion of $\text{AQH-CH}_2\text{CN}$ to AQ and CH_3CN before electron injection.

Fig. 1 shows the cyclic voltammograms of AQ and $\text{AQH-CH}_2\text{CN}$ in deaerated acetonitrile. In contrast to the reversible cyclic voltammogram of AQ (Fig. 1a), the cyclic voltammogram of $\text{AQH-CH}_2\text{CN}$ shows an irreversible redox wave (Fig. 1b), suggesting that the one-electron reduction of $\text{AQH-CH}_2\text{CN}$ was associated with an irreversible process (*vide infra*). The one-electron reduction potential of $\text{AQH-CH}_2\text{CN}$ was then determined as $E_{\text{red}}^0 = -1.10 \text{ V}$ (vs. Ag/Ag⁺) using differential pulse voltammetry (Fig. 1c), which is +0.15 V higher than the one-electron reduction potential of AQ [$E_{\text{red}}^0 = -1.25 \text{ V}$ (vs. Ag/Ag⁺)]. Not surprisingly, $\text{AQH-CH}_2\text{CN}$ containing the central sp^3



Scheme 2 (a)–(e) Concept of a one-electron switch: (a) electron injection into a host/guest(1) system yields a one-electron reduced species of guest(1) [guest(1)^{•-}]. (b) Guest(1)^{•-} spontaneously converts to guest(2)^{•-} associated with a release of a stable coproduct. (c) Electron transfer from guest(2)^{•-} to guest(1) occurs to yield a neutral guest(2) and guest(1)^{•-}, where guest(2) forms a host–guest complex [guest(2) ⊂ host]. (d) and (e) Sustainable electrocatalytic chain reactions convert all guest(1) into guest(2) to generate the guest(2) ⊂ host complexes.

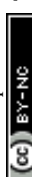


Scheme 1 (a) One-electron reduction of $\text{AQH-CH}_2\text{CN}$ -initiated CH_3CN release through electrocatalytic chain reactions. ORTEP view (50% probability) of $\text{AQH-CH}_2\text{CN}$. Hydrogen atoms are omitted for clarity. (b) Redox potentials of AQ and $\text{AQH-CH}_2\text{CN}$ in the electrocatalytic chain reaction. (c) Catalytic electron turns-on complex formation between AQ and $\text{U}_\text{H}\text{Ant}_2$ through sustainable electrocatalytic chain reactions.

carbon finds it rather difficult to accept an electron. Indeed, the optimized structure [DFT/UB3LYP-6-31G+(d,p)] of $\text{AQH-CH}_2\text{CN}^{\bullet-}$ suggests that the electron density of the singly occupied molecular orbital (SOMO) is low at the central sp^3 carbon (Fig. 1d), while the SOMO orbital of $\text{AQ}^{\bullet-}$ is fully delocalized across the entire molecule (Fig. 1e). Consequently, the SOMO energy level of $\text{AQH-CH}_2\text{CN}^{\bullet-}$ is 0.55 eV (12.7 kcal mol⁻¹) higher than that of $\text{AQ}^{\bullet-}$. Conversely, a fully dissociated state (*i.e.*, $\text{AQ}^{\bullet-} + \text{CH}_3\text{CN}$) is 1.39 eV (32.1 kcal mol⁻¹) lower than $\text{AQH-CH}_2\text{CN}^{\bullet-}$ (Fig. 1f).^{25,26} Therefore, the coupling of the dissociation of CH_3CN to the one-electron reduction of $\text{AQH-CH}_2\text{CN}$ (inset of Fig. 1c) should result in a significant shift of its one-electron reduction potential to the positive direction.

Using electron spin resonance (ESR) spectroscopy, we then detected the product after electron injection to $\text{AQH-CH}_2\text{CN}$ by addition of 1 equivalent of sodium naphthalenide ($\text{Np}^{\bullet-} \cdot \text{Na}^+$).²⁷ The ESR spectrum for $\text{AQ}^{\bullet-}$ was observed, which is identical to that obtained by the one-electron reduction of AQ (Fig. 1g vs. Fig. 1h), while no $\text{AQH-CH}_2\text{CN}^{\bullet-}$ species was detected (Fig. 1g).

With these results, we then obtained the UV/Vis absorption spectra of $\text{AQH-CH}_2\text{CN}$ with applied voltages of -0.8 , -1.0 , and -1.5 V (vs. Ag/Ag⁺) [Fig. 2a–c, respectively]. When the voltage of -0.8 V (vs. Ag/Ag⁺) was continuously applied to $\text{AQH-CH}_2\text{CN}$, no spectral change was observed (Fig. 2a). However, when the potential of -1.0 V (vs. Ag/Ag⁺) was applied to $\text{AQH-CH}_2\text{CN}$, UV/Vis absorption spectral changes were clearly observed with several isosbestic points (Fig. 2b). The resulting UV/Vis absorption spectrum after 290 s of applied voltage of -1.0 V



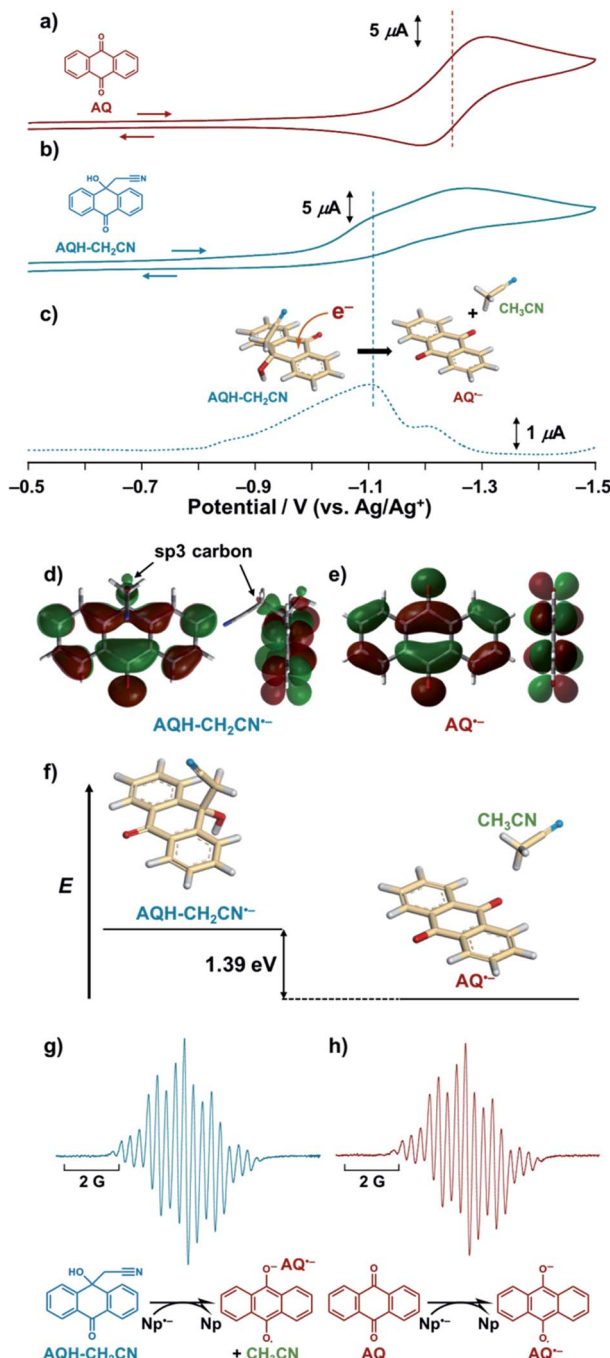


Fig. 1 (a) and (b) Cyclic voltammograms and (c) differential pulse voltammograms of (a) AQ (1.0×10^{-3} M) and (b) and (c) AQH-CH₂CN (1.0×10^{-3} M) in deaerated acetonitrile containing 0.1 M TBAP. Scan rate is 200 mV s⁻¹ (d) and (e) SOMO orbital for the optimized structures [DFT/UB3LYP-6-31G+(d,p)] of (d) AQH-CH₂CN⁻ and (e) AQ⁻. (f) Energy difference [DFT/UB3LYP-6-31G+(d,p)] between AQH-CH₂CN⁻ and its dissociated state (AQ⁻ + CH₃CN). ESR spectra of (g) AQH-CH₂CN (1.0×10^{-3} M) and (h) AQ (1.0×10^{-3} M) in the presence of Np²⁺. Na⁺ (1.0×10^{-3} M) in deaerated acetonitrile. Inset: (c) schematic representation of the one-electron reduction of AQH-CH₂CN coupling with dissociation of CH₃CN.

(vs. Ag/Ag⁺) is identical to that of AQ (Fig. 2b red line vs. Fig. 2d), suggesting a quantitative conversion of AQH-CH₂CN to AQ (AQH-CH₂CN \rightarrow AQ + CH₃CN), while no UV/Vis absorption

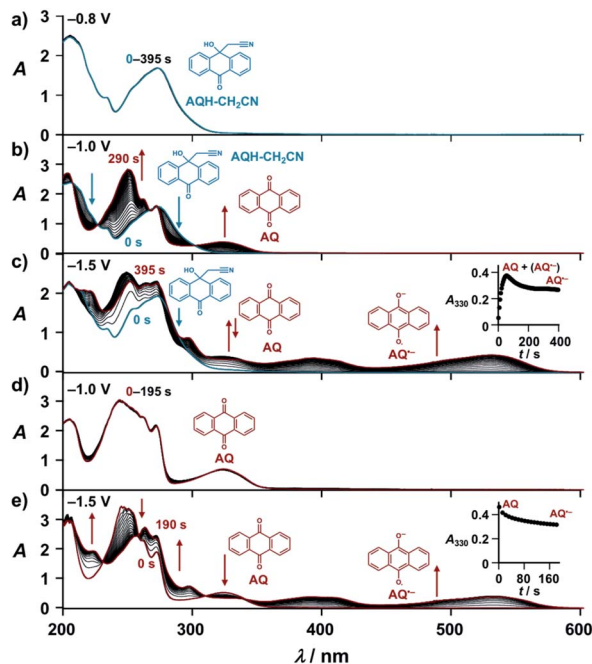
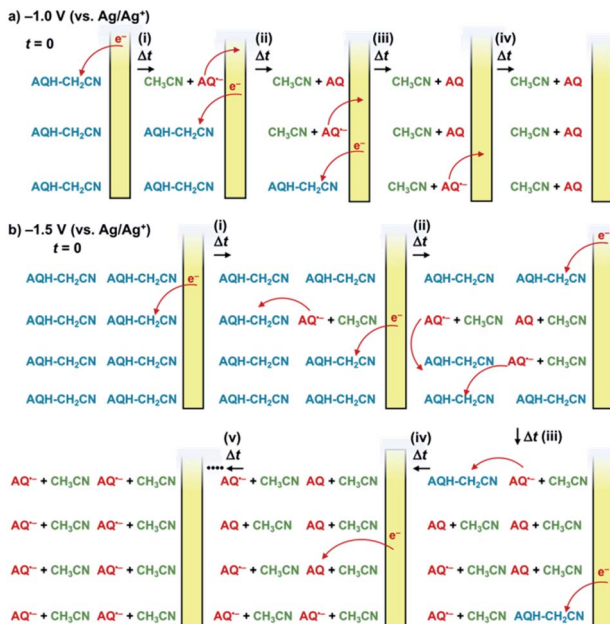


Fig. 2 (a)–(e) UV/Vis absorption spectra of (a)–(c) AQH-CH₂CN (1.0×10^{-3} M) and (d) and (e) AQ (1.0×10^{-3} M) under applying potentials of (a) -0.8 V, (b) and (d) -1.0 V, (c) and (e) -1.5 V (vs. Ag/Ag⁺) in deaerated acetonitrile containing 0.1 M TBAP (1 mm cuvette). Insets: (c) and (e) corresponding time course at $\lambda = 330$ nm.

bands due to AQ⁻ were observed (Fig. 2b). The one-electron oxidation potential of AQ⁻ [$E_{\text{ox}}^0 = -1.25$ V (vs. Ag/Ag⁺)] is lower than the applied potential [-1.0 V (vs. Ag/Ag⁺)], leading to rapid electron transfer to the working electrode and conversion of the temporarily generated AQ⁻ to AQ (Fig. 3a). In fact, the current flow was very low under these conditions (Fig. S3†).²⁸ No UV/Vis absorption spectral change took place for AQ under the -1.0 V (vs. Ag/Ag⁺) voltage (Fig. 2d), which is much higher than its one-electron reduction potential [$E_{\text{red}}^0 = -1.25$ V (vs. Ag/Ag⁺)]. Conversely, AQ was quantitatively converted to AQ⁻ under the more negative applied potential of -1.5 V (vs. Ag/Ag⁺) [Fig. 2e]. Then, the -1.5 V (vs. Ag/Ag⁺) potential was applied to AQH-CH₂CN, where AQH-CH₂CN also exhibited UV/Vis absorption spectral changes (Fig. 2c). The UV/Vis absorption spectrum of AQH-CH₂CN after 395 s of applied voltage of -1.5 V (vs. Ag/Ag⁺) is identical to that of AQ⁻ (Fig. 2c red line vs. Fig. 2e), suggesting that AQH-CH₂CN was directly converted to AQ⁻ (i.e., AQH-CH₂CN + e⁻ \rightarrow AQ⁻ + CH₃CN) in this case. Here, the absorbance at 330 nm (due to AQ) increased upon applying the voltage of -1.5 V (vs. Ag/Ag⁺) to AQH-CH₂CN at $t = 0$ –55 s, after which the absorbance decreased and reached saturation at $t = 395$ s (inset of Fig. 2c). The reactant of AQH-CH₂CN gave no appreciable absorption at 330 nm ($\epsilon_{300}^{\text{AQH-CH}_2\text{CN}} \approx 0$), and the molar absorption coefficient of AQ was larger than that of AQ⁻ at 330 nm ($\epsilon_{300}^{\text{AQ}} > \epsilon_{300}^{\text{AQ}^-}$, inset of Fig. 2e). Hence, the initial increase and the subsequent decrease of absorbance observed at 330 nm (inset of Fig. 2c) indicated temporary generation of AQ and its subsequent conversion into AQ⁻ as explained below. Because the applied voltage of -1.5 V (vs. Ag/Ag⁺) is sufficiently



lower than the one-electron oxidation potential of $\text{AQ}^{\cdot-}$ [$E_{\text{ox}}^0 = -1.25$ V (vs. Ag/Ag^+)], no further electron transfer to the electrode was expected (Fig. 3b(i)). The resulting $\text{AQ}^{\cdot-}$ [$E_{\text{ox}}^0 = -1.25$ V (vs. Ag/Ag^+)] has sufficient reducing power to reduce $\text{AQH-CH}_2\text{CN}$ [$E_{\text{red}}^0 = -1.10$ V (vs. Ag/Ag^+)], generating the secondary $\text{AQ}^{\cdot-}$, while the original $\text{AQ}^{\cdot-}$ was oxidized to AQ (Fig. 3b(ii)). Conversely, $\text{AQH-CH}_2\text{CN}$ is easier to be reduced than AQ , and hence $\text{AQH-CH}_2\text{CN}$ will more preferentially undergo one-electron reduction by the electrode than the subsequently formed AQ . In addition, chain electron transfer from $\text{AQ}^{\cdot-}$ to $\text{AQH-CH}_2\text{CN}$ also takes place to increase the concentration of AQ around the surface of the working electrode (Fig. 3b(i)–(iv)). When all the $\text{AQH-CH}_2\text{CN}$ molecules were consumed, the AQ molecules generated by the electrocatalytic chain reactions started to be reduced by the electrode (Fig. 3b(v)).

The electrocatalytic chain reaction was initiated by chemical reduction of $\text{AQH-CH}_2\text{CN}$ (5.0×10^{-2} M) using only 0.1 equivalent of $\text{Np}^{\cdot-}\cdot\text{Na}^+$ (5.0×10^{-3} M) in deaerated THF (Fig. 4 and ESI Movie S1†). Before addition of $\text{Np}^{\cdot-}\cdot\text{Na}^+$, the THF solution of $\text{AQH-CH}_2\text{CN}$ was colorless and transparent; however, upon addition of $\text{Np}^{\cdot-}\cdot\text{Na}^+$ (0.1 eq.), the solution color immediately turned red (Fig. 4b to c). The resulting red color corresponds to $\text{AQ}^{\cdot-}$, whose red color was confirmed by electrochemical reduction of AQ (Fig. 4a). Then, the solution was suspended for 10 min after the $\text{Np}^{\cdot-}\cdot\text{Na}^+$ addition, and the reaction was complete within 60 min under these conditions. The red color arising from $\text{AQ}^{\cdot-}$ was maintained during the reaction (Fig. 4d and S4†). The resulting yellow precipitate was AQ that was not completely soluble in THF under the high concentration conditions employed ($[\text{C}]_0 = 5.0 \times 10^{-2}$ M).

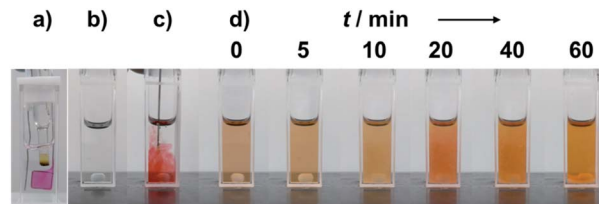


Fig. 4 (a) Photograph of the cuvette after electrochemical reduction of AQ . (b)–(d) Photographs of a deaerated THF solution containing $\text{AQH-CH}_2\text{CN}$ (5.0×10^{-2} M) (b) before addition, (c) upon addition, and (d) after addition of $\text{Np}^{\cdot-}\cdot\text{Na}^+$ (5.0×10^{-3} M) at 0–60 min.

The CH_3CN generated during the electrocatalytic chain reactions was monitored by NMR spectroscopy (Fig. 5). Upon introduction of 0.1 equivalent of $\text{Np}^{\cdot-}\cdot\text{Na}^+$ (2.0×10^{-3} M) into $\text{AQH-CH}_2\text{CN}$ (2.0×10^{-2} M) in deaerated THF-d_8 , ^1H NMR signals corresponding to $\text{AQH-CH}_2\text{CN}$ (blue triangles) gradually decreased and a concomitant increase of signals arising from the formation of AQ (red circles) and CH_3CN (green triangles) was observed (Fig. 5a and S5†). The corresponding time course curves (Fig. 5b) showed that the initial 20 mM of $\text{AQH-CH}_2\text{CN}$ (blue triangles) was almost completely consumed at $t =$

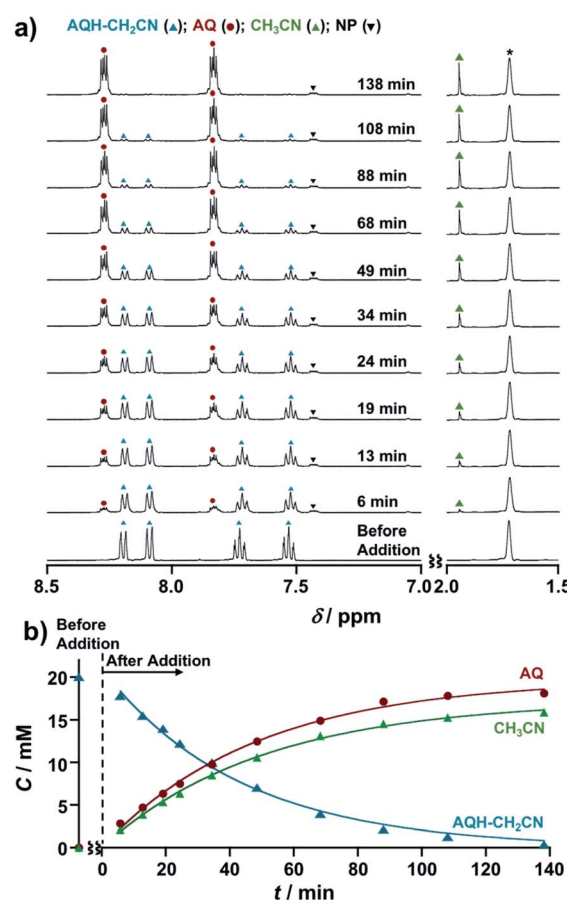


Fig. 5 (a) ^1H NMR spectra of $\text{AQH-CH}_2\text{CN}$ (2.0×10^{-2} M) upon addition of $\text{Np}^{\cdot-}\cdot\text{Na}^+$ (2.0×10^{-3} M) in THF-d_8 . Signal denoted by an asterisk is from the solvent. The intensity of the spectra at 1.5–2.0 ppm is scaled vertically (1/2) for clarity. (b) Corresponding time course.



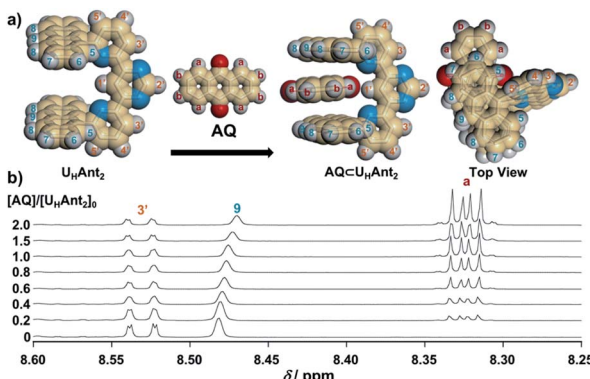


Fig. 6 (a) Optimized structures [DFT/CAM-B3LYP-6-31G(d)] of U_HAnt_2 and $\text{AQ} \subset \text{U}_\text{HAnt}_2$. (b) Stacked ^1H NMR spectra (for H^{3'}, H⁹, and H^a) of U_HAnt_2 (3.5 \times 10 $^{-3}$ M) in the presence of AQ (0–7.0 \times 10 $^{-3}$ M) in CDCl_3 .

138 min, where the formation of AQ (red circles) and the associated CH_3CN released (green triangles) reached saturation.²⁹

In light of these results, we can summarize the electrocatalytic chain reaction (Scheme 1) as follows: at the initial step, electron injection to $\text{AQH-CH}_2\text{CN}$ produces $\text{AQ}^\cdot-$, with the process driven by bond breaking associated with proton migration. The initially formed $\text{AQ}^\cdot-$ can subsequently reduce the $\text{AQH-CH}_2\text{CN}$ reactant to generate secondary $\text{AQ}^\cdot-$ and CH_3CN , while the initial $\text{AQ}^\cdot-$ is oxidized to AQ (Scheme 1a). Then, the secondary-formed $\text{AQ}^\cdot-$ is also capable of reducing the reactant of $\text{AQH-CH}_2\text{CN}$ to generate a next $\text{AQ}^\cdot-$ associated with the concomitant release of CH_3CN (Scheme 1a). Thus, conversion of $\text{AQH-CH}_2\text{CN}$ to AQ and CH_3CN is the electrocatalytic chain reaction process mediated by $\text{AQ}^\cdot-$ (Scheme 1a). The electrocatalytic chain reactions are terminated when all the $\text{AQH-CH}_2\text{CN}$ is consumed, while the concentration of $\text{AQ}^\cdot-$ remains unchanged during the chain reaction. If the present electrocatalytic chain reaction mechanism is valid, the rates of the concentration changes ($|dC/dt|$) of AQ, CH_3CN , and $\text{AQH-CH}_2\text{CN}$ would obey pseudo-first-order kinetics because the observed rate ($|dC/dt|$) can be represented as $k_{\text{et}}[\text{AQ}^\cdot-][C]$, where the $[\text{AQ}^\cdot-]$ term is constant during the chain reaction. This was confirmed by time course curves obtained from the above ^1H NMR kinetics experiments, where each time course obeyed first-order kinetics with very similar pseudo-first-order rate constants ($k_{\text{obs}} = k_{\text{et}}[\text{AQ}^\cdot-] = 3.3\text{--}3.9 \times 10^{-4} \text{ s}^{-1}$) [Fig. 5b]. The observed reaction rate also increased with an increase in the initial concentration of the added $\text{Np}^\cdot-\cdot\text{Na}^+$ (i.e., $[\text{Np}^\cdot-\cdot\text{Na}^+]_0 = [\text{AQ}^\cdot-]$) [Fig. S6†]. Therefore, we can extract the electron-transfer rate constant ($k_{\text{et}} = 1.6\text{--}1.9 \times 10^{-1} \text{ M}^{-1} \text{ s}^{-1}$) by using the initial concentration of $\text{Np}^\cdot-\cdot\text{Na}^+$ (2.0 \times 10 $^{-3}$ M). The determined k_{et} value ($k_{\text{et}} = 1.6\text{--}1.9 \times 10^{-1} \text{ M}^{-1} \text{ s}^{-1}$) is reasonable for slightly exergonic electron transfer with a large reorganization energy arising from the bond breaking/proton migration.³⁰ Moreover, the conversion of $\text{AQH-CH}_2\text{CN}$ to AQ and CH_3CN can be completed only with 0.025 equivalent of $\text{Np}^\cdot-\cdot\text{Na}^+$ used as the initiator (Fig. S7†), suggesting that the turnover number of the electrocatalytic chain reactions is at least greater than 40.

As the present electrocatalytic chain reactions were mild and sustainable, we investigated their application to CT interaction turn-on systems (*vide infra*). Electron donor host compound U_HAnt_2 , first synthesized by Lehn *et al.*, was used for this purpose.³¹ U_HAnt_2 bears anthracene tweezers suitable for insertion of a planar electron-acceptor molecule to form a stable D-A-D-type CT complex.³¹ The possibility of CT complex formation between U_HAnt_2 and AQ was predicted by DFT modeling [DFT/CAM-B3LYP-6-31G(d)], which suggested that D-A-D-type CT complex formation ($\text{AQ} \subset \text{U}_\text{HAnt}_2$) was reasonable (Fig. 6a and S8†). Furthermore, the ^1H NMR spectrum of U_HAnt_2 showed that anthracene aromatic protons (H⁷, H⁸, and H⁹) were shifted upfield upon addition of AQ (Fig. 6b and S9–S13†). This observation was consistent with the stacked D-A-D CT model comprising anthracene rings shielded by the central anthraquinone plane (Fig. 6a). The electrocatalytic conversion of $\text{AQH-CH}_2\text{CN}$ to AQ was then examined by applying a potential of -1.0 V (vs. Ag/Ag^+) to $\text{AQH-CH}_2\text{CN}$ in the presence of U_HAnt_2 . The absorption band resulting from AQ formation was successfully observed, along with the appearance of a broad absorption band at around 410 nm (Fig. 7a). Successive addition of AQ to U_HAnt_2 resulted in appearance of the same broad absorption band in a longer wavelength region (Fig. S14†). Conversely, both U_HAnt_2 alone and AQ alone showed no absorption band in this longer wavelength region (Fig. S15 and S16†). Time-dependent (TD) DFT of $\text{AQ} \subset \text{U}_\text{HAnt}_2$ indicated that the newly observed broad absorption band was attributed to the CT transition from the anthracene tweezers to the inserted central AQ molecule (Fig. 7b). Further assignment of the CT

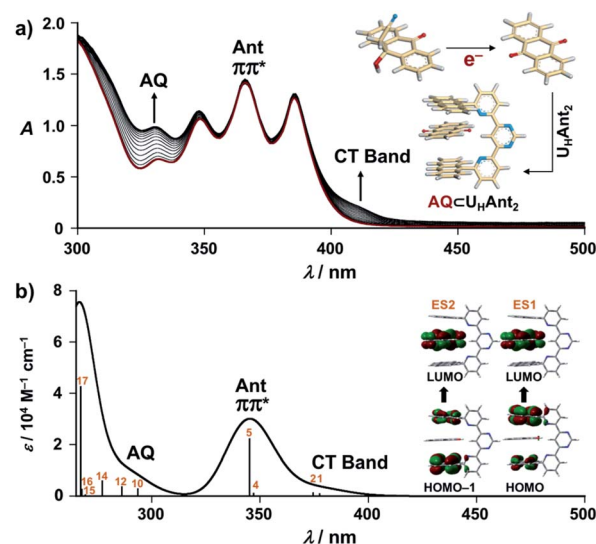


Fig. 7 (a) UV/Vis absorption spectra of $\text{AQH-CH}_2\text{CN}$ (8.0 \times 10 $^{-4}$ M) in the presence of U_HAnt_2 (8.0 \times 10 $^{-4}$ M) under applying a potential of -1.0 V (vs. Ag/Ag^+) (0–395 s) in deaerated THF containing 0.1 M TBAP (1 mm cuvette). (b) Calculated UV/Vis absorption spectrum [TD-DFT/CAM-B3LYP-6-31G(d), IEFPCM:THF] of the optimized structure of $\text{AQ} \subset \text{U}_\text{HAnt}_2$ [DFT/CAM-B3LYP-6-31G(d), IEFPCM:THF]. Insets: (a) schematic representation of CT complex formation turned on by the catalytic electron. (b) Summary of excited states 1 and 2.



band was performed with quinones having different one-electron reduction potentials (see details in Fig. S17–S20†). During the electrocatalytic conversion, $U_{\text{H}}\text{Ant}_2$ showed no degradation (Fig. 7a). Besides, DFT and electrochemical studies (Fig. S8, S21 and S22†) revealed that the mediator $\text{AQ}^{\cdot-}$ (reduced form) has no interaction with $U_{\text{H}}\text{Ant}_2$, enabling the sustainable electrocatalytic chain reaction even in the presence of $U_{\text{H}}\text{Ant}_2$. In contrast, a mixture of $U_{\text{H}}\text{Ant}_2$ and $\text{AQH-CH}_2\text{CN}$ provided no CT absorption band (Fig. S23†), suggesting no effective CT interaction between them. Reactant $\text{AQH-CH}_2\text{CN}$ is a non-planar molecule containing several sp^3 carbon atoms, making it unsuitable for CT interaction with the anthracene tweezers of $U_{\text{H}}\text{Ant}_2$. Furthermore, the CT interactions could also be turned on by electrocatalytic conversion of $\text{AQH-CH}_2\text{CN}$ to AQ initiated by chemical reduction using $\text{Np}^{\cdot-}\cdot\text{Na}^+$ (Fig. S24†). Therefore, the CT interactions could be turned on by electrocatalytic conversion of $\text{AQH-CH}_2\text{CN}$ to AQ for CT complex ($\text{AQ} \subset U_{\text{H}}\text{Ant}_2$) formation (Scheme 1c; inset of Fig. 7a).³²

Conclusions

In conclusion, we successfully demonstrated the electron injection-triggered solvent (CH_3CN) molecular release associated with formation of a redox active quinone derivative (AQ) through sustainable electrocatalytic chain reactions. The presented electrocatalytic chain reactions enable guest molecular release and should be mild enough to apply to a wide range of host–guest systems. This study reports a first example of successful catalytic electron-triggered CT complex formation. These findings provide new opportunities for creating a “one-electron switch” (Scheme 2) in association with catalytic electrons as the input dots to trigger specific molecular recognition.

Author contributions

Y. O. and S. I. performed the synthesis and characterization of materials, and also contributed the titration experiments. D. O. contributed the analysis of the experimental data. J. Y. designed the study, analysed the experimental data and wrote the manuscript.

Conflicts of interest

There are no conflicts to declare.

Acknowledgements

This work was partly supported by JSPS KAKENHI, Grant Numbers: JP19H02693, JP19K22207, and JP21H05404 in Scientific Research on Innovative Areas “Dynamic Exciton”, a Grant-in-Aid for the ASAHI Glass Foundation, and the Iketani Foundation. We thank Iain Mackie, PhD, and Simon Partridge, PhD, from Edanz (<https://jp.edanz.com/ac>) for editing a draft of this manuscript.

Notes and references

- (a) A. Studer and D. P. Curran, *Nat. Chem.*, 2014, **6**, 765; (b) A. Studer and D. P. Curran, *Angew. Chem., Int. Ed.*, 2016, **55**, 58.
- M. A. Syroeshkin, F. Kuriakose, E. A. Saverina, V. A. Timofeeva, M. P. Egorov and I. V. Alabugin, *Angew. Chem., Int. Ed.*, 2019, **58**, 5532.
- C. Costentin, M. Robert and J.-M. Saveant, *Chem. Phys.*, 2006, **324**, 40.
- M. A. Syroeshkin, I. B. Krylov, A. M. Hughes, I. V. Alabugin, D. V. Nasybullina, M. Y. Sharipov, V. P. Gulyai and A. O. Terent'ev, *J. Phys. Org. Chem.*, 2017, **30**, e3744.
- X. Tang and A. Studer, *Angew. Chem., Int. Ed.*, 2018, **57**, 814.
- M. Vacher, I. F. Galvan, B.-W. Ding, S. Schramm, R. Berraudo-Pache, P. Naumov, N. Ferre, Y.-J. Liu, I. Navizet, D. Roca-Sanjuan, W. J. Baader and R. Lindh, *Chem. Rev.*, 2018, **118**, 6927.
- D. Davis, V. P. Vysotskiy, Y. Sajeev and L. S. Cederbaum, *Angew. Chem., Int. Ed.*, 2012, **51**, 8003.
- (a) A. Studer and D. P. Curran, *Angew. Chem., Int. Ed.*, 2011, **50**, 5018; (b) S. Zhou, G. M. Anderson, B. Mondal, E. Doni, V. Ironmonger, M. Kranz, T. Tuttle and J. A. Murphy, *Chem. Sci.*, 2014, **5**, 476; (c) J. P. Barham, G. Coulthard, R. G. Kane, N. Delgado, M. P. John and J. A. Murphy, *Angew. Chem., Int. Ed.*, 2016, **55**, 4492.
- J. Kim, D. J. Darley, W. Buckel and A. J. Pierik, *Nature*, 2008, **452**, 239.
- M. Majek and A. Jacobi von Wangenheim, *Angew. Chem., Int. Ed.*, 2015, **54**, 2270.
- J. Du, K. L. Skubi, D. M. Schultz and T. P. Yoon, *Science*, 2014, **344**, 392.
- Similar situations can be found in oxidant upconversion, where hole catalysis has been utilized as an alternative input to induce the isomerization of photochromic compounds, see: (a) T. Nakashima, Y. Kajiki, S. Fukumoto, M. Taguchi, S. Nagao, S. Hirota and T. Kawai, *J. Am. Chem. Soc.*, 2012, **134**, 19877; (b) S. Lee, Y. You, K. Ohkubo, S. Fukuzumi and W. Nam, *Chem. Sci.*, 2014, **5**, 1463; (c) A. Goulet-Hanssens, C. Rietze, E. Titov, L. Abdullahu, L. Grubert, P. Saalfrank and S. Hecht, *Chem.*, 2018, **4**, 1740.
- J. Yuasa and S. Fukuzumi, *J. Am. Chem. Soc.*, 2007, **129**, 12912.
- (a) V. Croue, S. Goeb, G. Szaloki, M. Allain and M. Salle, *Angew. Chem., Int. Ed.*, 2016, **55**, 1746; (b) G. Szaloki, V. Croue, V. Carre, F. Aubriet, O. Aleveque, E. Levillain, M. Allain, J. Arago, E. Orti, S. Goeb and M. Salle, *Angew. Chem., Int. Ed.*, 2017, **56**, 16272.
- (a) D. Ogata and J. Yuasa, *Angew. Chem., Int. Ed.*, 2019, **58**, 18424; (b) Y. Imai and J. Yuasa, *Chem. Sci.*, 2019, **10**, 4236; (c) K. Hamashima and J. Yuasa, *Angew. Chem., Int. Ed.*, 2022, **61**, e202113914.
- M. Han, R. Michel, B. He, Y.-S. Chen, D. Stalke, M. John and G. H. Clever, *Angew. Chem., Int. Ed.*, 2013, **52**, 1319.
- S. Hiraoka, K. Harano, M. Shiro and M. Shionoya, *Angew. Chem., Int. Ed.*, 2005, **44**, 2727.



18 L. S. Lisboa, J. A. Findlay, L. J. Wright, C. G. Hartinger and J. D. Crowley, *Angew. Chem., Int. Ed.*, 2020, **59**, 11101.

19 After we submitted this manuscript, Stoddart *et al.* reported an important and excellent example, which also underlined the importance of an electron as a catalyst (trigger) of molecular recognition, see: Y. Jiao, Y. Qiu, L. Zhang, W.-G. Liu, H. Mao, H. Chen, Y. Feng, K. Cai, D. Shen, B. Song, X.-Y. Chen, X. Li, X. Zhao, R. M. Young, C. L. Stern, M. R. Wasielewski, R. D. Astumian, W. A. Goddard III and J. F. Stoddart, *Nature*, 2022, **603**, 265.

20 C. C. Moser, J. M. Keske, K. Warnecke, R. S. Farid and P. L. Dutton, *Nature*, 1992, **355**, 796.

21 S. Iseki, K. Nonomura, S. Kishida, D. Ogata and J. Yuasa, *J. Am. Chem. Soc.*, 2020, **142**, 15842.

22 (a) D. P. August, G. S. Nichol and P. J. Lusby, *Angew. Chem., Int. Ed.*, 2016, **55**, 15022; (b) V. Martí-Centelles, A. L. Lawrence and P. J. Lusby, *J. Am. Chem. Soc.*, 2018, **140**, 2862.

23 S. Sugiura and H. Maeda, *Chem. Commun.*, 2021, **57**, 6983.

24 S. M. Lukonina, S. V. Mikhailova, I. K. Korobeinicheva, v. A. Loskutov and E. P. Fokin, *Russ. Chem. Bull.*, 1983, **32**, 2379.

25 The free energy change ($|\Delta G_{\text{rxn}}^{\cdot-}|$) of radical-anionic version of the fragmentation should be much smaller in the real system (see details in Fig. S1†).

26 Although the detailed mechanism of the fragmentation of acetonitrile in $\text{AQH-CH}_2\text{CN}^{\cdot-}$ could not be established, DFT study indicates that the fragmentation is likely to be triggered by the intramolecular proton transfer (see details in Fig. S2†).

27 Y. Inui, S. Miyazaki, K. Ohkubo, S. Fukuzumi and T. Kojima, *Angew. Chem., Int. Ed.*, 2012, **51**, 4623.

28 Accurate determination of the coulombic efficiency could be difficult in this system, because the current flow was extremely low under the potential of -1.0 V (vs. Ag/Ag^+) (Fig. S3†).

29 The remaining (ungenerated) 2 mM of AQ should still exist as $\text{AQ}^{\cdot-}$ formed by the initial electron transfer from $\text{Np}^{\cdot-}\cdot\text{Na}^+$ to $\text{AQH-CH}_2\text{CN}$. Conversely, undetected remaining CH_3CN may result from volatilization.

30 J. Yuasa, S. Yamada and S. Fukuzumi, *J. Am. Chem. Soc.*, 2008, **130**, 5808.

31 A. Petitjean, R. G. Khoury, N. Kyritsakas and J.-M. Lehn, *J. Am. Chem. Soc.*, 2004, **126**, 6637.

32 The titration experiment indicated that the binding constant (K_{CT}) between $\text{U}_\text{H}\text{Ant}_2$ and AQ is 140 M^{-1} (Fig. S25†).

